Jurnal Teknologi Reaktor Nuklir

Tri Dasa Mega

Journal homepage: jurnal.batan.go.id/index.php/tridam

Estimation of Neutron and Prompt Photon Dose Rate Distribution in TMSR-500 Using MCNP6

Luqman Satria Pradana[1*], Utari[1], Suharyana[1], Azizul Khakim[2]

[1]*Physics Department, Faculty of Mathematics and Natural Sciences, Universitas Sebelas Maret, Jl. Ir. Sutami No. 3A Kentingan, Jebres, Surakarta – Central Java, Indonesia 57126*
[2]*Research Center for Nuclear Reactor Technology, Research Organization for Nuclear Energy, National Research and Innovation Agency, Building No. 80, BJ Habibie Science and Technology Research Center, Serpong, Banten, Indonesia 15314*

ARTICLE INFO

Article history:

Received:15 September 2022
Received in revised form:19 October 2022
Accepted:25 October 2022

Keywords:

Neutron and Prompt Photon
Dose Rate Distribution
MCNP6
TMSR-500

A B S T R A C T

Thorium Molten Salt Reactor-500 (TMSR-500), one of the Generation IV nuclear reactors, is designed by Thorcon International, Pte. Ltd, which is projected to be built in Indonesia. The reactor core is radially surrounded by B_4C shielding, but not the upper part. As the silo hall sits above the reactor core and is accessible by reactor personnel, the dose rate must be calculated in the area to ensure the workers receive an annual dose below the acceptable limit. The dose rate from neutrons and photons as the result of fission reactions are the only sources to be calculated in this research, without taking the source from fission products into account. This research aims to obtain the dose rate distribution of neutrons and prompt photons using Monte Carlo code MCNP6. The reactor was assumed to operate at a nominal thermal power of 557 MWth. Dose rate calculation was obtained from flux Tally F4 and converted into dose rate using Dose Energy Dose Function (DEDF) factor. Conversion factors of flux to the dose were based on ICRP-21 and ANSI/ANS-6.1.1 1977. The result of the calculations showed that the distribution of neutron and prompt photon fluxes does not reach the silo hall.

1. INTRODUCTION

Molten Salt Reactor (MSR) is one of Generation IV nuclear reactors which uses molten salt serving as both coolant and fuel. The molten salt consists of liquid coolant (commonly fluoride salt, which is used as a coolant in fluoride salt-cooled high-temperature reactors) and fuel (fissile and fertile material)[1]. MSR design normally uses multi-loop coolants. Primary coolant commonly uses uranium fuel dissolved in sodium fluoride, while the secondary coolant uses sodium fluoride. There are several advantages of liquid fuel over solid fuel, such as the fuel acting simultaneously as coolant and allowing separation of fission products (FPs) while the reactor operates [2].

*Corresponding author
Email: luqmanpradana@gmail.com
DOI: 10.17146/tdm.2022.24.3.6692

Oak Ridge National Laboratory (ORNL) proposed the first MSR design to power military aircraft. As a result of national policy decisions, this program was terminated. The ORNL design was adapted into civilian nuclear power program. The research focused on the development of fuel sustainability using thermal spectrum-based $^{232}Th/^{233}U$ cycle. From 1965 to 1969, the Molten Salt Reactor Experiment (MSRE) was operated using ^{235}U and ^{233}U without thorium in a single fluid design. MSRE demonstration was successful and showed the MSR design reliability. The concept of MSRE led to the Molten Salt Breeder Reactor (MSBR) design, which used fluoride coolant, thorium, and uranium. The breeding ratio was estimated to be 1.06, indicating the potential mixture of coolant, uranium, and thorium as fuel salt [1].

In terms of fuel composition, Thorium Molten Salt Reactor (TMSR-500) has a similarity with MSBR, which used ^{232}Th as fertile material to produce ^{233}U as fissile material. TMSR-500 fresh fuel salt consists of NaF-BeF_2-ThF_4-$^{238}UF_4$-$^{235}UF_4$ composed of 76/12/9.5/2.0/0.5 percent mole, respectively. Fuel salt is located in the reactor core, called as Pot in the TMSR-500 design. The design of TMSR-500 has 4 Pots in which a single Pot can generate 557 MWth or 250 MWe for four years. The core will be refueled continuously while the reactor is operating [3].

Reactor design should ensure a proper radiation protection for the workers, public, and the environment. The Nuclear Energy Regulatory Agency of Indonesia (BAPETEN) establishes an effective dose limit for workers of 100 mSv for five years (accumulative) [4]. TMSR-500 is the first MSR nuclear power plant design planned to be built in Indonesia. This research aims to obtain and provide information on neutron and prompt photon dose distribution in the Silo Hall area where workers can access the area and are close to the location of the Pot.

TMSR-500 Silo Hall is modeled and calculated using Monte Carlo N-Particle version 6 (MCNP6) code. MCNP6 is capable of simulating the interaction of neutrons, photons, and electrons with matter by employing Monte Carlo method. As the primary sources of dose radiations from nuclear reactors come from neutrons and gamma rays (photons), the code fits the need for estimating the dose distribution surrounding the reactor. In addition, dose conversion factors of neutron and photon radiations are available in the code. MCNP6 has been benchmarked and widely used by nuclear researchers in many applications. In this research, we estimate that the dose is only resulted from neutron and prompt photon emission regardless of fission products. As for the latter, additional depletion calculation has to be done by applying continuous "feed and bleed" for four years of operation which requires expensive computational resources. In addition to the need for many time steps for burnup calculation, MCNP does not provide a feature for continuous fuel feeding and removal. Therefore, this research is limited to estimating the dose at the beginning of reactor life where the fuel is fresh, and no fission product has been generated.

2. THEORY

Neutron Sources in Reactor

A fission nuclear reactor has a neutron source to initiate a fission reaction. Neutron sources can be classified into two types, intrinsic neutron sources and installed neutron sources. The reactor can produce neutrons through several interactions called intrinsic neutron sources, for example, decay of heavy nuclide ($^{235}_{92}$U, $^{238}_{92}$U, $^{239}_{94}$Pu, $^{240}_{94}$Pu) and reaction involving natural boron and fuel. This source always occurs in radioactive materials. Neutrons produced from radionuclide decay are called delayed neutrons. The reactors use installed neutron sources to initiate the initial fission reaction and maintain the availability of neutrons in the reactor because intrinsic neutron sources are relatively weak and depend on the recent power history of the reactor. Commonly, the location of this source is in or close to the reactor. An example of installed neutron sources is $^{252}_{98}$Cf which can undergo spontaneous fission [5, 6].

Some interactions produce neutrons, such as radionuclide reaction (α,n), fission reaction, and photo-neutron reaction. Radionuclide reaction is a reaction between the alpha emitter and light elements. Beryllium ($^{9}_{4}$Be) is most often used for neutron source, and the alpha emitter is polonium ($^{210}_{84}$Po) as shown in Eq. 1 [7].

$$^{9}_{4}\mathrm{Be} + \alpha \rightarrow {}^{12}_{6}\mathrm{C} + n \quad (1)$$

A fission reaction occurs when a heavy nuclide (fissile material) absorbs a neutron and becomes an unstable nuclide. To achieve stability, it splits into two large fragments and emits 2-3 neutrons as described by Eq. 2 [8]. Interaction of gamma-ray and deuterium is another neutron source as illustrated in Eq. 3. This neutron source is called photo-neutron because the interaction of electromagnetic radiation produces a neutron [5].

$$^{235}_{92}\mathrm{U} + n \rightarrow {}^{236}_{92}\mathrm{U} \rightarrow {}^{140}_{55}\mathrm{Cs} + {}^{93}_{37}\mathrm{Rb} + 3\,n \quad (2)$$

$$^{2}_{1}\mathrm{H} + \gamma \rightarrow {}^{1}_{1}\mathrm{H} + n \quad (3)$$

The spectrum energy of neutron can be classified into three regions, namely thermal (0<E<0.625 eV), intermediate (0.625 eV<E<0.5 MeV), and fast (E>0.5MeV). Fast neutrons are produced from fission reaction, whereas thermal and intermediate neutrons are results of neutron interaction with reactor materials, in form of slowing down process [9].

Neutron interactions can be either scattering or absorption. Scattering interactions are classified into elastic and inelastic scattering, whereas absorption interactions are classified into radiative capture, fission reaction, and particle ejection[6].

Photon Sources in Reactor

Photon sources can be classified into two types, prompt photon and delayed photon. Neutron interactions with materials can produce photons called prompt photons. A primary prompt photon is

a photon produced from neutron-material interactions. Several types of neutron interactions with materials can produce photon (γ-rays), such as fission reaction, radiative capture, and inelastic scattering. A secondary prompt photon is a photon that is produced from a primary prompt photon interaction with materials, such as the photoelectric effect and Compton scattering. Delayed photons originate from radionuclide decay and activation products. Other source of photon are from bremsstrahlung reaction and positron annihilation [10].

Photon-material interactions differ from particle-material interactions because of the absence of mass and charge, and therefore its interactions are through indirect ionization. Depending on photon energy, there are three photon-material interactions, photoelectric effect (<0.2 MeV), Compton scattering (0.2 MeV< E <1.02 MeV), and pair production (E > 1.02 MeV) [6].

Neutron Flux

Neutrons and photons emitted to all directions in the nuclear reactor area. The number of neutrons that travel in one cm^3 is called neutron density (n, neutron/cm^3). The length of travel distance of these neutrons per second depends on their velocity (v, cm^2/s). To obtain the intensity of neutrons per cm^2 per second by multiplying neutron density and v (in this case, for monoenergetic neutron). This intensity is called flux (ϕ, neutron/cm^2-s) as described by Eq. 4.

$$\phi = n\,v \tag{4}$$

Radiation Dose

The dose can be classified into three types: absorbed dose (D), equivalent dose, and effective dose (E). Absorbed dose represents the amount of imparted energy per unit mass and does not distinguish the type of radiation particle. Equivalent dose is the product of absorbed dose and radiation weighting factor (W_R). The radiation particle and its energy determine the value of weighting factor. Effective dose represents equivalent dose in tissues or organs with a different weighting factor. Obtaining effective dose is by multiplying the appropriate tissue or organ weighting factor (W_T) with the equivalent dose. The dose rate indicates the amount of doses received at a particular time scale [11].

Thorium Molten Salt Reactor

TMSR-500 operates using 2 Pots to generate 500 MWe. Besides Pot, inside the Can, there are Primary Heat Exchanger (PHX), Primary Loop Pump (PLP), and 2 Off Gas Recuperators (OGR) as shown in Fig. 1. The Can is located inside the Silo Hall area or Fission Island 14 m below the ground surface and submerged in the water. It helps cool down the Can, aside from using a tube wall (water piped surrounding the Can) to transfer the heat [3].

There are several gamma radiation shieldings, such as Can lid gamma shielding, borated water, and two gamma shielding above and below borated water as shown in Fig. 3. In the radial direction, B_4C is installed as a shielding to absorb the neutron leakage as shown in Fig. 1 [3].

The reactor core consists of a central log, fuel salt log, reflector, and boron carbide shielding. The central log consists of 3 control rods (Gd_2O_3) and a regulating rod (graphite). The absorber control rods are fully withdrawn when the reactor is operating, on the other hand the graphite regulating rod is fully inserted. Fuel salt flows through gaps in the fuel salt log, which is a graphite-based moderator [3].

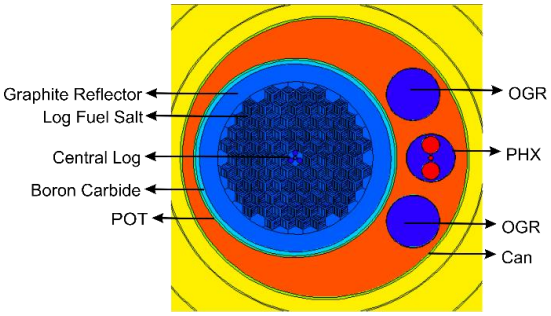

Fig. 1. Axial Cross Section Inside the Can

3. METHODOLOGY

This research aims to obtain and provide information on neutron and prompt photon distribution in the Silo Hall area. The research flow chart is depicted in Fig. 2.

Geometrical Model

The core geometry has been modeled that includes the Can, submerged Silo Hall, a rad tank (borated water), the worker access area, and the ground. This study only considered a single Pot or reactor core of the TMSR-500. The gamma shielding was assumed to be made of lead. There were six chosen artificial tallied cells located at different axial positions i.e., two sample cells inside the Can, one sample in Submerged Silo Hall, one in borated water, one in the worker area, and one in the ground as shown in Fig. 3. The tallied samples will provide the value of neutron and prompt photon flux and dose rate.

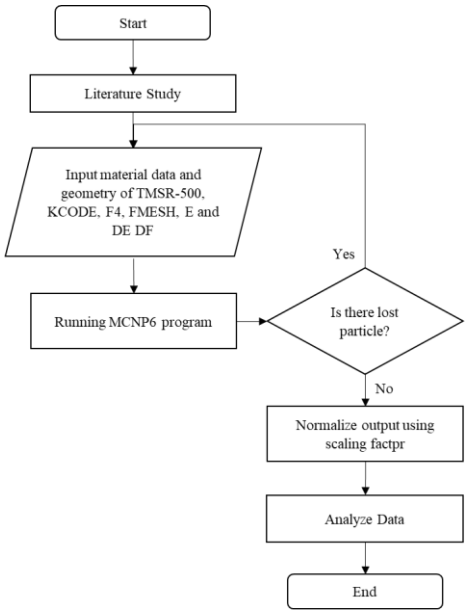

Fig. 2. Research Flow Chart

Criticality Calculation (k_{eff})

For criticality calculation, KCODE card was applied. To produce sufficiently small deviation, 200000 particles were simulated for 300 cycles, where the first 50 cycles were skipped. After the first 50 cycles, it can be assured that all tallies and k_{eff} have been stable.

Flux Calculation

Tally F4 estimates flux average over a defined cell (particle/cm^2) [12]. However, the code also provides tally F4 for an arbitrary undefined cells by using FMESH4 (particles/cm^2) at a desired user location [13].

Flux to Dose Rate Conversion

Converting flux to dose rate requires a conversion factor of Dose Energy (DE) and Dose Function (DF). In this calculation, ICRP-21 and ANSI/ANS-6.1.1 1977 conversion factors were chosen and compared for identifying the more conservative results. Those conversion factors were chosen because they provide the data of equivalent dose rate for neutron and photon available in the current version of MCNP code.

Scaling Factor

For KCODE calculation, the MCNP tallies (including tally F4) are produced per one fission neutron generation. In order to obtain the absolute values, the tally outputs have to be multiplied by a scaling factor (SF). The scaling factor is defined by Eq. 5 [12].

$$SF = \frac{P\,v}{1.6022\ \text{x}\ 10^{-13}.\ k_{eff}\ .\ w_f} \qquad (5)$$

where,

P	:	reactor power (Watt)
v	:	average neutrons produced per fission
k_{eff}	:	multiplication factor
w_f	:	energy released per fission (MeV)
1.6022 x 10^{-13}	:	MeV to Joule conversion

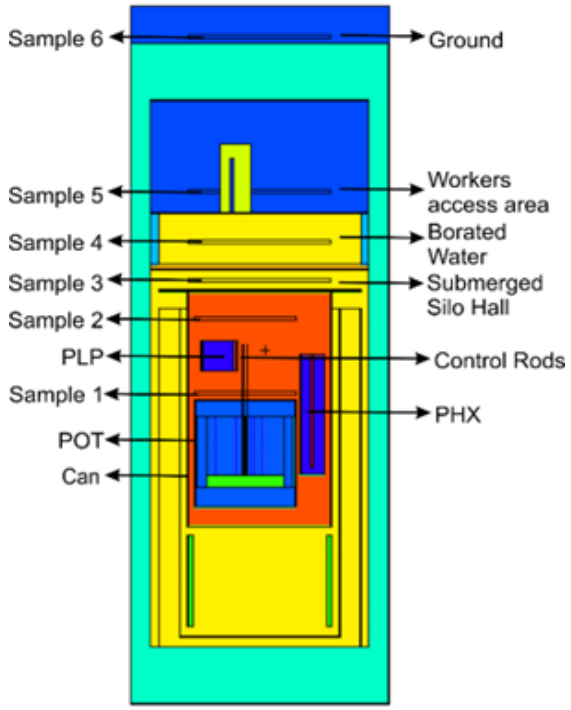

Fig. 3. Sample and design of TMSR-500

Fig. 3 shows the MCNP6 geometrical model on sample locations and levels to be tallied above the reactor Pot.

4. RESULT AND DISCUSSION

The obtained calculation is a statistical estimate that simulates the characteristics of neutron and photon. The result of MCNP6 simulations confirmed that neutron fluxes were detected in two samples (samples 1 and 2), whereas the prompt photon fluxes were found in three samples (samples 1, 2, and 3). The tallied fluxes will be converted to dose rate (Sv/h). The flux and dose rate were then normalized using a scaling factor of 4.19 × 10^{19} neutron/s calculated from Eq. 5.

Neutron Energy Spectrum on Samples

Fig. 4. exhibits a similar neutron energy spectra in Sample 1 and Sample 2. The spectrum confirm that TMSR-500 is a thermal reactor where fission reactions are dominated by thermal neutrons. The contributions of fission reactions caused by thermal, intermediate, and fast neutrons are 93.2%, 6.39%, and 0.42%, respectively. This has also been confirmed by A. Khakim [14]. As the control rod absorbers are positioned above the core, they absorb the neutron flux in the axial direction. In addition, as sample 2 is located farther from the core than the Sample 1, the flux of Sample 2 is lower than that of Sample 1.

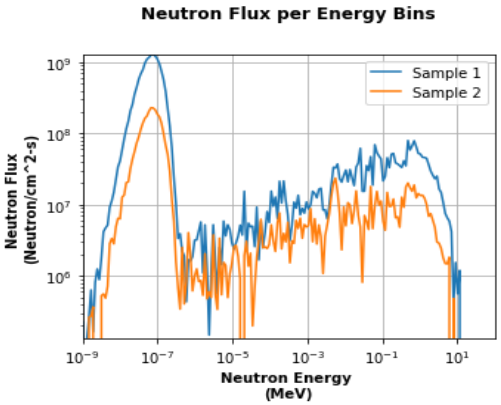

Fig. 4. Neutron Flux Energy Distribution

Three dimensions (3-D) neutron flux distribution of Sample 1 and 2 are shown in Fig. 5. In Sample 1, the distribution of neutrons looks like a dome with a basin in the middle as shown in Fig. 5. As we know, the radiation will be emitted to all directions, but the flux produces the dome-shaped neutron distribution. It is due to effect of B_4C that absorbed the neutrons which spread to the radial axis. Control rods that absorb the neutrons, affecting the dome-shaped distribution with a basin in the middle. The neutron flux distribution in Sample 2 is different from that in Sample 1. The distribution of neutrons dominated at positive X-axis (X > 0 cm) as shown in Fig. 5. This is due to neutron travel from the pot without being blocked by any materials or components. While at negative X-axis (X < 0 cm), PLP blocked neutron path.

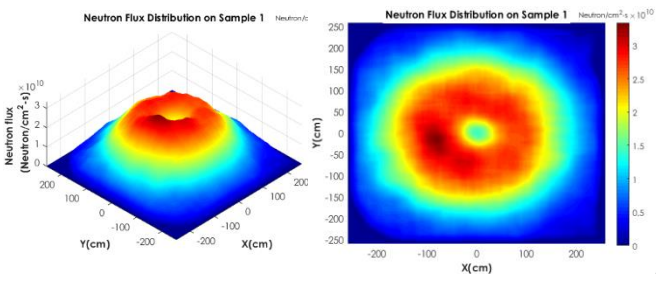

(a) (b)

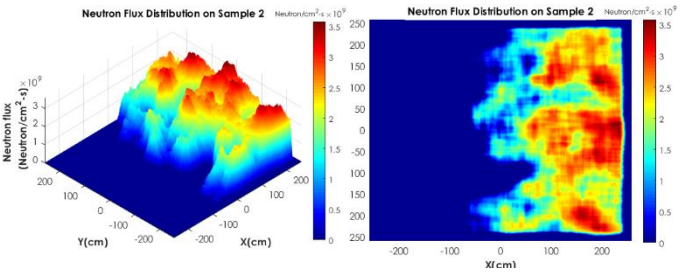

(c) (d)

Fig. 5 Neutron Flux Distribution (a) visualization on sample 1 in 3D, (b) visualization on sample 1 XY axis, (c) visualization on sample 2 in 3D, and (d) visualization on sample 2 XY axis.

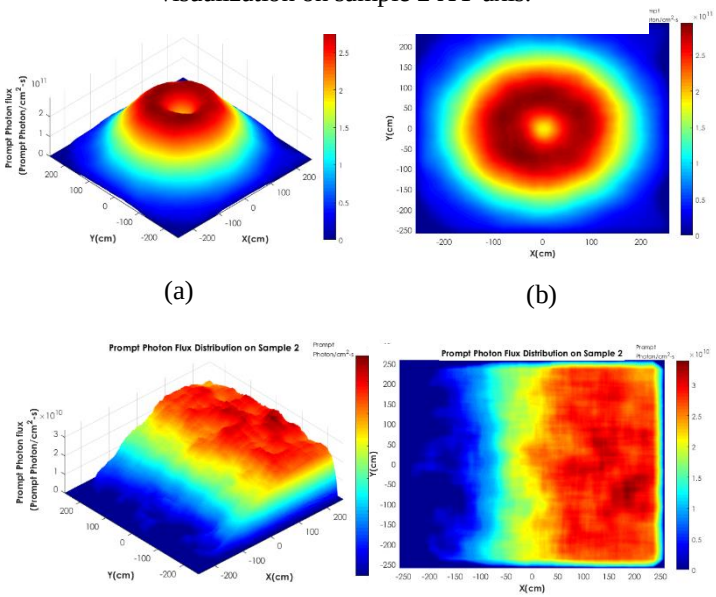

(a) (b)

(c) (d)

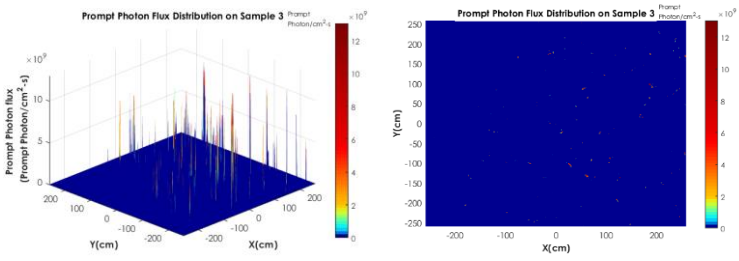

(e) (f)

Fig. 6. Prompt Photon Flux Distribution (a) visualization on sample 1 in 3D, (b) visualization on sample 1 XY axis, (c) visualization on sample 2 in 3D, (d) visualization on sample 2 XY axis, (e) visualization on sample 3 in 3D, and (f) visualization on sample 3 XY axis.

Prompt Photon Flux Distribution on Samples

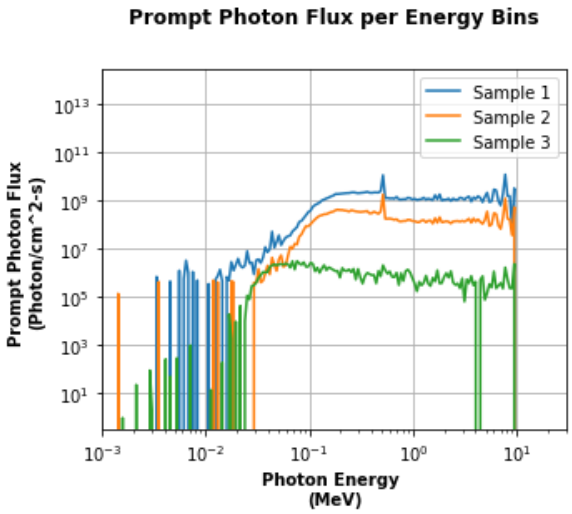

Fig.7. Prompt Photon Flux Energy Distribution

Fig. shows prompt photon energy spectrum distribution in samples 1, 2, and 3. Sample 1 and Sample 2 are inside the Can, which contains helium gas, while Sample 3 is outside the Can (in Submerged Silo Hall). Samples 1 and 2 have a similar trend, while Sample 3 is slightly different from two other samples. That is caused by Can Lid Gamma Shielding over the Can.

The prompt photon at Samples 1 and 2 were not much different from neutron. In Sample 1, the interactions of fast neutron with control rods (Gd_2O_3) can produce gamma ray [15]. So, in its surrounding area, prompt photons are produced more than in other areas. 3-D visualization also shows a basin in the middle of the dome because of prompt photons production due to neutron-material interactions as shown in Fig. 6.

In Sample 2, the distribution of prompt photons is similar to neutron distribution but more even as shown in Fig. 6. This is because the source of prompt photons comes from neutron-material interaction and subsequent photon-material interactions, so the population of the prompt photon is more than neutrons.

Prompt photon still can penetrate through the Can Lid Gamma Shielding over the Can, approximately 0.54%. It shows that lead can reduce photon and proves lead's capability as gamma shielding.

Axial Distribution of Neutron and Prompt Photon Flux

The axial flux distributions were calculated using FMESH from above the Pot to ground (± 1974.5 cm above the Pot). Five coordinates to calculate neutron and photon flux (for all energy range) in x and y axis are (0,0); (172.7,0); (-172.7,0); (0, -172.7); and (0,172.7). Neutron flux was detected until ± 880 cm above the pot whereas prompt photons flux was detected until ± 970 cm above the pot.

Fig. shows neutron flux distribution in each height at five points. The dark blue line (0,0) location is ± 86 cm above the graphite moderator. So, more neutron flux is detected here than at other points. When neutrons travel close into the control rods, neutron flux decreases due to absorption by the control rods.

The red line shows an increase in neutron flux at (-172.7,0) when entering PLP as shown in Fig. . The PLP contains fuel salt, where fission reaction may take place that increases neutron flux. At PLP, the fission chain reactions do not last long because there is no moderator, which result in decrease of neutron flux.

At point (172.7,0), the green line shows neutron flux decrease to be more stable than at other points. Neutrons travel to the axial direction without being blocked by any material around that point. Meanwhile, the point at (0,172.7) cyan line and (0, -172.7) purple line, neutron flux decreases caused by the points close to the PLP. The differences in neutron flux at three points occur when neutrons are at the height of 426 cm or through the height of the PLP as shown in Fig. . It shows that material can generally affect the population of neutrons depending on the cross-section.

The profile of axial prompt photon flux distribution exhibits a similar pattern as shown in Fig. . The maximum prompt photon flux is generated at the top of the core where the neutron flux is high. It decreases gradually until the PLP, then measured at zero as it passes through the PLP.

At the level where a 5 cm-thick Can lid gamma shield is installed, the photon radiation decreases drastically due to attenuation as shown Fig. . In submerged Silo Hall (water), prompt photons are still detected until it is absorbed by gamma shielding 1 (above the submerged Silo Hall). At a height ± 970 cm (above gamma shielding 1), prompt photon was not detected anymore.

Lead Characteristics as Gamma Shielding

Photon that interacts with matter can produce a subsequent photon. This research detects subsequent photon production by the photoelectric effect, Compton scattering, and annihilation. Prompt photon energy on Can Lid Gamma Shielding is more evenly distributed than Gamma Shielding 1, even though they have a similar trend. As it passes through the water, photon radiation was undetectable due to water attenuation and distance.

Photon-material interactions depend on the energy of the photon. A photon with energy range of 10^{-3} to 10^{-1} MeV is more likely to interact with matter through photoelectric effect. When the energy of a photon has the same energy as binding energy for each Pb shell, the atom absorbs that energy, and the electron are ejected from the atom. Due to a vacancy in the inner shell, an electron from outer shell enters the inner shell. The transition of electron is emitting characteristic x-rays. Energies of x-rays equal to the difference in binding energy between initial and final shells ($E_x = E_i - E_f$). The population of the photon with these energies (E_x) increases so that photon flux peaks (K, L, and M) are formed as shown in Fig. . The trend of photon flux peak formed on lead is the same as the trend of lead testing using x-ray fluorescence (XRF) device as shown in Fig.10 [16]. Table 1 shows energy binding in K, L, and M shells for Pb.

Compton scattering occurs in photons with energies 10^{-2} MeV up to 1.02 MeV. Photon transfers energy to electron in the outer shell, so the energy of the photon decreases. The effect of this phenomenon will increase the photon flux with

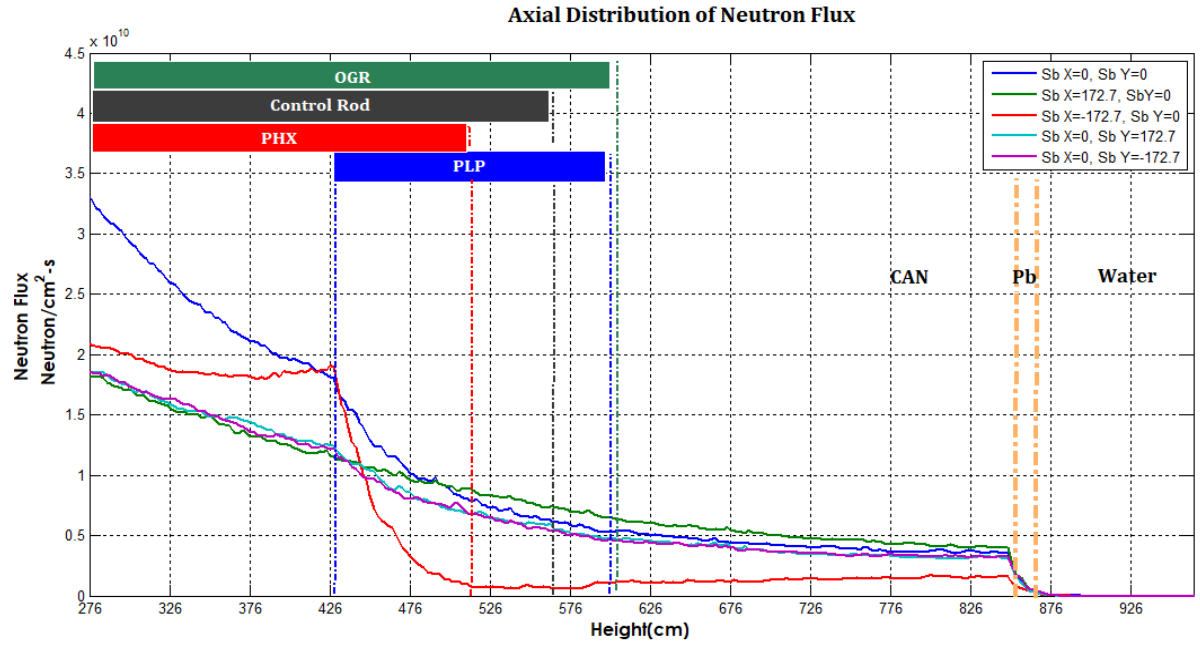

(a)

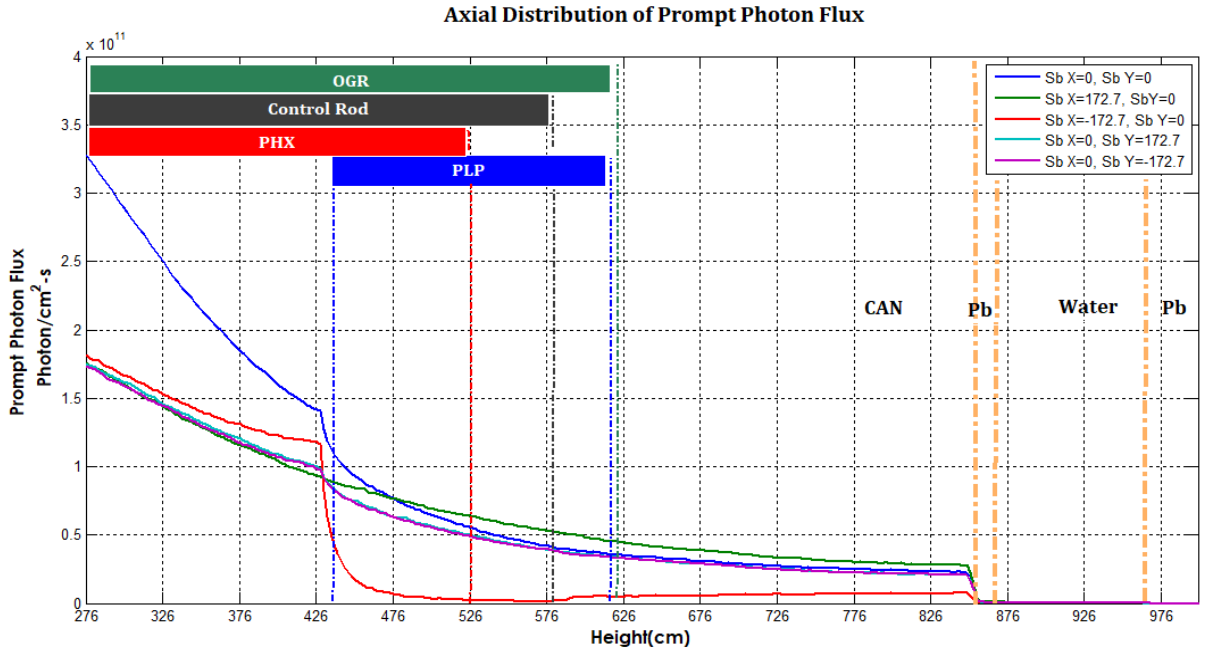

(b)

Fig. 8. (a) Neutron and (b) Prompt photon flux on axial distribution

energies under 10^{-2}. Fig. shows prompt photon flux with energies under 10^{-2} MeV at Sample 2 (orange line) is relatively low than Sample 1 (blue line). At Sample 3 (green line), the prompt photon flux with energies under 10^{-2} MeV increases. It occurs because of the effect of Compton scattering that produces photon with energies under 10^{-2} MeV and the photoelectric effect that produces x-ray fluorescence on Can Lid Gamma Shielding.

Another photon production is annihilation. It occurred when positron and electron, each with energy ± 0.51 MeV, collapsed and formed two gamma rays with an energy of 0.51 MeV

Table 1. Shells binding energy in lead

Shell	Binding Energy (eV)
K	88011
L_1	15867
L_2	15206
L_3	13041
M_1	3857
M_2	3560
M_3	3072
M_4	2592
M_5	2490

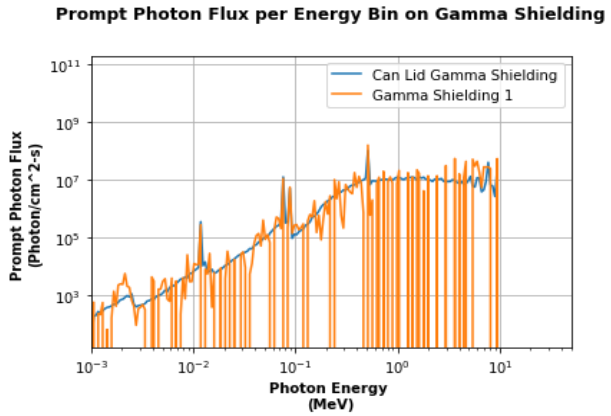

Fig. 9. Prompt photon flux energy on gamma shielding

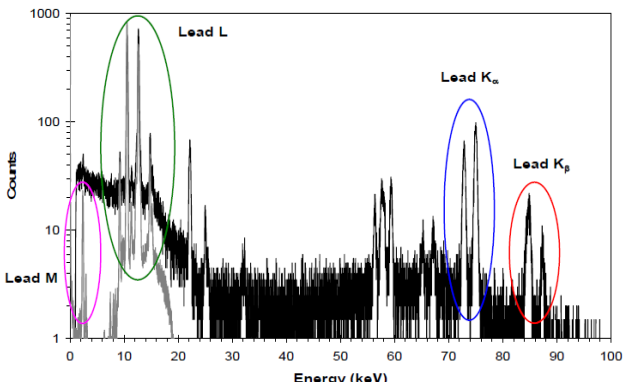

Fig.10. X-Rays fluorescence in lead [16]

Dose Rate Comparison using ICRP-21 and ANSI/ANS-6.1.1 1977 Conversion

Radiation dose will be detected when there are radiation particles, and the magnitude depends on the flux particle and energy. ICRP-21 and ANSI/ANS-6.1.1 1977 dose rate conversions are slightly different for neutron and photon. The maximum difference between the two conversion factors for neutron and photon are 4% and 15%, respectively, as shown in Table 2 and Table 3. Table 2 presents the neutron dose rate estimation at Sample 1 and Sample 2 using ICRP-21 and ANSI/ANS-6.1.1-1977 conversion factors. Dose rate is not detected at Sample 3

Table 2. Neutron Dose Rate Estimation

Neutron Dose Rate			
Sample	ICRP-21 (Sv/h)	ANSI/ANS-6.1.1-1977 (Sv/h)	Diff (%)
Sample 1	1.74×10^{3}	1.79×10^{3}	3
Sample 2	3.80×10^{2}	3.97×10^{2}	4

Table 3 presents the prompt photon dose rate estimation at various sample locations using ICRP-21 and ANSI/ANS-6.1.1-1977 conversion factors.

Table 3. Prompt Photon Dose Rate Estimation

Prompt Photon			
Sample	ICRP-21 (Sv/h)	ANSI/ANS-6.1.1-1977 (Sv/h)	Diff (%)
Sample 1	4.26×10^{3}	4.62×10^{3}	8
Sample 2	5.17×10^{2}	5.67×10^{2}	9
Sample 3	1.52	1.76	15

ANSI/ANS-6.1.1-1977 consistently produces higher dose rate both for neutron and photon as compared to ICRP-21. In addition, both conversion factors exhibit smaller differences for high dose rates. Overall, ANSI/ANS-6.1.1-1977 conversion factor is more conservative in term of safety consideration, as it produces higher dose rate than ICRP-21.

5. CONCLUSION

Based on the calculation result using MCNP6, neutron and prompt photon do not reach the workers area above the rad tank, so no dose rate is detected in that area. It shows that water and lead gamma shield effectively reduce neutrons and prompt photon flux. The neutron was detected ± 20 cm above rad tank (in submerged Silo Hall) after penetrating Can Lid. At the same time, the

effectiveness of lead material in reducing prompt photon flux is approximately 99%. It is obtained by comparing the dose rate at Sample 2 and Sample 3 even though there is prompt photon travelling through helium and water.

In this study, ANSI/ANS-6.1.1 1977 is more conservative than ICRP-21 for flux to dose rate conversion. The difference between two conversions increases when the dose rate value is small. In radiation protection consideration, a more conservative conversion is preferable to estimate the maximum dose for the workers and the public.

AUTHOR CONTRIBUTIONS

All authors contributed equally in this paper. All authors reviewed and agreed the final version of the manuscript.

REFERENCES

1. Gehin J.C., Powers J.J. Liquid Fuel Molten Salt Reactors for Thorium Utilization. Nucl. Technol. 2016. **194**(2):152–61.
2. Buckthorpe D. Introduction to Generation IV Nuclear Reactors. Struct. Mater. Gener. IV Nucl. React. 2017.:1–22.
3. Devanney J., Jorgensen L., Livingston J., Moir R., Rodenburg A.C., Uhlik C. ThorCon the Do-able Molten Salt Reactor Design Control Document. 2015.
4. BAPETEN Peraturan Kepala Badan Pengawas Tenaga Nuklir Repulik Indonesia. Perka BAPETEN. 2013. **4 Thn 2013**:1–29.
5. Ji R.M., Yu C.G., Li M.H., Yan R., Zou Y., Liu G.M. Study on Inherent Neutron Sources in MSR. Nucl. Sci. Tech. 2018. **29**(4)
6. Schön J.H. Nuclear/Radioactive Properties. 2015.
7. Obodovskiy I. Neutron Sources. Radiation. 2019.:289–92.
8. De Sanctis E., Monti S., Ripani M. Energy from Nuclear Fission: An Introduction. Cham:Springer International Publishing AG; 2016.
9. Al Zain J., El Hajjaji O., El Bardouni T., Boukhal H. Deterministic Evaluation of Safety Parameters and Neutron Flux Spectra in the MNSR Research Reactor using DRAGON-4 code. J. Radiat. Res. Appl. Sci. 2018. **11**(3):255–61.
10. Nguyen T.S., Wang X., Yue S. Validations of Gamma Measurements in Research Reactors With MCNP Full-Reactor Models. CNL Nucl. Rev. 2017.:1–7.
11. Fisher D.R., Fahey F.H. Appropriate Use of Effective Dose in Radiation Protection and Risk Assessment. Health Phys. 2017. **113**(2):102–9.
12. Rook J.C., Weber K.P., Corcoran E.C. Advanced MCNP Simulation of the Neutron and Photon Flux and Absorbed Dose Rates for the SLOWPOKE-2 Nuclear Reactor at the Royal Military College of Canada. Nucl. Technol. 2020. **206**(12):1861–74.
13. Erawati Fadli O., Suparmi S., Khakim A., Suharyana S., Riyatun R. Power and Neutron Flux Distribution Analysis in the RSG-GAS Reactor :Preliminary Study to Identify the Reactor Readiness as Power Ramp Test Facility (PRTF). J. Phys. Conf. Ser. 2019. **1153**(1)
14. Khakim A., Rhoma F., Waluyo A., Suharyana S. The neutronic Characteristics of Thermal Molten salt Reactor. AIP Conf. Proc. 2021. **2374**
15. İrim G., Wis A.A., Keskin M.A., Baykara O., Ozkoc G., Avcı A., et al. Physical, Mechanical and Neutron Shielding Properties of h-BN/Gd2O3/HDPE Ternary Nanocomposites. Radiat. Phys. Chem. 2018. **144**:434–43.
16. Amptek X-Ray Fluorescence (XRF): Understanding Characteristic X-Rays. 2016.:1–6.